Hydrothermal Synthesis and Electrochemical Characterization of Hexagonal Zr-CuS Nanocomposite and its Charge Storage Capacity

J. William Brown[1], D. Geetha[1,*], P.S. Ramesh[2] and Surekha Podili[1]

[1]Department of Physics, Annamalai University, Chidambaram-608002, India
[2]Department of Physics, Thiru Kolanjiappar Government Arts and Science College, Virudhachalam-606001, India

*Corresponding author: E-mail: geeramphyau@gmail.com

Hexagonal zirconia doped CuS nanaocomposites were successfully synthesized through a simple mild hydrothermal synthesis. The higher dopent concentration of zirconia produces increased mesoporous homogeneous nanostructures. The structure and nature of the resulting product (Zr-CuS) were characterized by XRD, XPS, SEM/EDS and TEM techniques. The results show that zirconia is homogeneously dispersed on CuS and well separated from one another. Electrochemical studies show that the final product (Zr-CuS) possesses high specific surface area. An increase in zirconia concentration might increase the mesopore volume and a widening of microporosity. Zirconia doped CuS composite exhibits high electrochemical performance with a high capacitance of 949.47 F g⁻¹. The presence of zirconia in CuS improves the capacitive behaviour of samples. Therefore, Zr-CuS could be promising nanocomposite for energy storage device.

Keywords: Zirconium, Copper sulphide, Nanaocomposites, Specific capacitance, Supercapacitor.

INTRODUCTION

The energy crisis has initiated novel research on the low cost, environmental friendly and renewable energy resources. Therefore, numerous efforts have been devoted to develop low cost electrode materials with superior electrochemical property [1]. Composite containing earth abundant copper and transition metals doped newer materials have intensively optimized and exhibit useful properties [2]. However, several metal sulfide nanoparticles with unique property have not yet been explored.

Zirconium is the first ceramic material well known for its abrasion, corrosion and heat as well as low brittleness. Zirconium sulfide (ZrS) is an attractive material in various applications due to its excellent textural properties as resistance, low cost, high density, mechanical, thermal, optical and electrical characteristics [3,4]. Nanocomposite containing inorganic metals exhibits different properties compared to individual component, in terms of chemical and physical properties which are much better too. Chraska *et al.* [5] reported that cubic ZrO_2 posses decent electrochemical properties due to its excellent electrical and surface charge properties and biocompatibity. Even though

it′s moderate redox behaviour and electrochemical active surface area [6], the individual component may not used be as electrode material for energy storage applications. Hence materials with high surface areas and good electrical conductivity can be potentially applied to improve the electro chemical properties of zirconium. In this regard, CuS has selected as base material to improve the electrochemical conductivity due to high mechanical flexibility and good stability.

Compared to individual components mixed metal sulfides provide better textural, chemical and physical properties than each individual component. These nanocomposites are extensively used in almost all energy storage and conversion devices [7]. In this study, zirconia-impregrated on copper sulfide nanocomposites were aimed to synthesize to improve their electrochemical properties. The effect of zirconia on CuS was studied using variety of techniques. Generally, hydrothermal method involve longer reaction period. The disadvantage of this process is that size and shape, which are difficult to control as they undergo rapid nucleation and growth. Lowering the reaction temperature and time can have significant effect on the growth process. Here an attempt has been made to synthesis zirconium-

CuS nanostructures at low hydrothermal temperature (130°C) and the reaction time is 10 h. In particular, nanocomposites were tested using cyclic voltammetry (CV) and electrical impedance spectroscopy (EIS) for their electrochemical response.

EXPERIMENTAL

The chemicals *viz.* copper nitrate trihydrate, ethylene glycol, thiourea, cetyltrimethylammonium bromide (CTAB)) and zirconium nitrate trihydrate were procured from Sigma-Aldrich and of high purity grade.

Synthesis of zirconium doped CuS: Ethylene glycol (40 mL) was used to dissolve 1 mM of copper nitrate trihydrate, 2 mM of thiourea and 0.1 mM of CTAB. Three proportions of zirconium precursor *viz.* 0.05, 0.15 and 0.30 mM were added and forceful stirring was performed for 45 min. The resultant compound was kept at 130 ºC for 10 h, which resulted in the formation of black colour precipitate and dried at 60 ºC for 6 h.

Characterization: X-ray diffraction (XRD) patterns were obtained with a Rigaku Ultima III diffractometer, equipped with a rotating anode and a Cu*K*α radiation source (λ = 0.15418 nm). FTIR determined the functional groups using a Perkin-Elmer spectrometer range from 4000-400 cm⁻¹. SEM scrutinized the surface morphology (JEOL-JSM 5610 LV with INCA EDS) and the elements were analyzed by EDS, in combination with SEM and TEM-CM-200. Electrochemical behaviour of CuS and Cd-CuS was examined in an electrochemical workstation (CHI 660C, USA) by cyclic voltammetry (CV) and electron impedance spectroscopy (EIS).

Electrochemical characterization: The electrochemical properties were characterized out using a standard three-electrode cell at room temperature (24±1 ºC) by using a computer controlled potentiostat (Princeton Applied Research, VSP). A saturated Ag/AgCl electrode and a platinum-coated titanium mesh (2.5 cm² in size) were used as reference and counter electrodes, respectively. A modified glassy carbon electrode (diameter 3 mm) was used as the working electrode and 2 M KOH as the electrolyte. The cyclic voltammograms were recorded between −1.3 and 1.1 V *vs.* Ag/AgCl at a scan rate 100 mV/s [8].

RESULTS AND DISCUSSION

Structural analysis: The powder XRD measurements for Zr-CuS are presented in Fig. 1(a-d), to examine the crystal structure of electrode material. The XRD pattern matched well with standard JCPDS Card no. 27-0997. A peak at 30º, which resulted in Zr and CuS precursors, it indicates the presence of tetragonal ZrS structure [9] and intense sharp peaks at (100), (101), (102),(103) and (006) for hexagonal covellite peaks, (JCPDS card No. 24-0060) [10]. The absence of impurity peaks in the spectrum clearly represents that the sample contains a pure cubic structure of Zr-CuS.

X-ray diffraction data for Zr-CuS indicates both tetragonal and monoclinic phases of ZrS₂ form. The average crystal sizes of Zr-CuS nanoparticles estimated using Debye-Scherrer equation [11] was about 15, 19 and 26 nm, respectively, which is further confirmed by TEM micrographs.
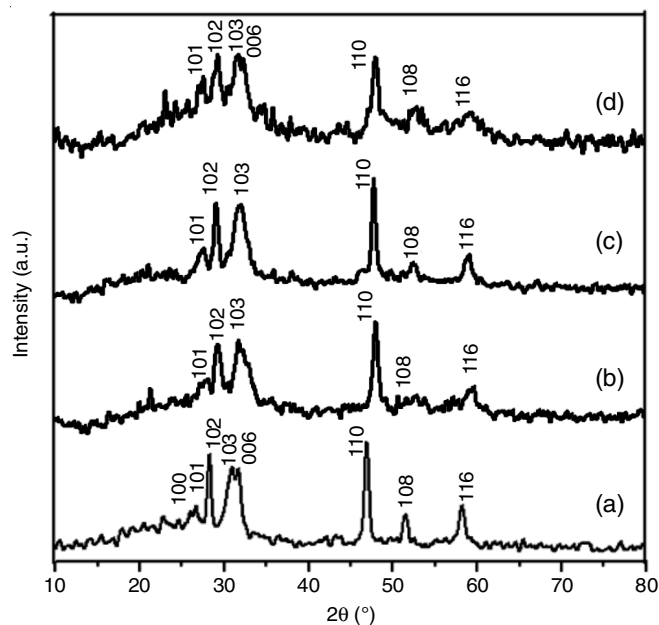

Fig. 1.   XRD Spectra of (a) CTAB stabilized CuS (b) Zr (0.05)-CuS (c) Zr (0.15)-CuS and (d) (0.30) Zr-CuS nanostrutures

XPS measurements: Surface compositions of Zr-CuS samples were analyzed by XPS technique which provided an information regarding the electronic states and chemical environment of zirconium, copper and sulfur atoms in the composite materials. Fig. 2(a-d) shows wide survey XP spectra in the full range of the binding energy , scanned from 0 to 1200 eV which provided both compositional overview and information about main elemental components in Zr-CuS. The Zr-CuS samples produced two different peaks, a strong peak between 184 and 178 eV for copper and other peaks were identified at 931.59 eV and 951.37 eV. The presence of Zr 3*d* and Zr 3*p* peaks was visualized. Analyzing the Zr 3*d*$_{5/2}$ region, a peak centered at 183 eV assigned to Zr⁴⁺ is obtained in stoichiometric Zr-CuS. Fig. 2d represents the S 2*p* spectrum of the sample. The peak located at a binding energy of 162.53 eV corresponds to Cu-S atom. Moreover, this assignation is confirmed by XRD results.

FTIR analysis: IR spectra of Zr-CuS nanocomposites are shown in Fig. 3a-d. For comparison, a spectrum of CTAB stabilized CuS before Zr was doped and also presented. As expected, a large difference was confirmed between CuS and Zr doped CuS. The intense broad peaks between 700-600 cm⁻¹ assigned to the S=O or S-O bond are the characteristic peaks. Also the fine structure splitting of IR spectra disappears. Only the broad bands between 1100 and 650 cm⁻¹ are attributed to the sulphated vibration modes. Thus, sulfated Zr-Cu can more easily transform on to glass electron in its surface according to the bifunctional mecahism [12]. A broad curve in the range 3500-3000 cm⁻¹ is due to bending vibration of H₂O. A triplet observed at 1397, 1125 and 1099 cm⁻¹ is due to asymmetric stretching of carbonyl (C =O) group. The band at 1610 cm⁻¹ is for OH bending of water. The observed results are in concurrence with the earlier report [13]. The peaks at 606 and 729 cm⁻¹ signify the existence of Zr²⁺ doped CuS bond [14]. The cubic phase of Zr-CuS exhibits intense absorption bands in the range of 850-500 cm⁻¹, which are attributed to the Zr-S bond [15]. In
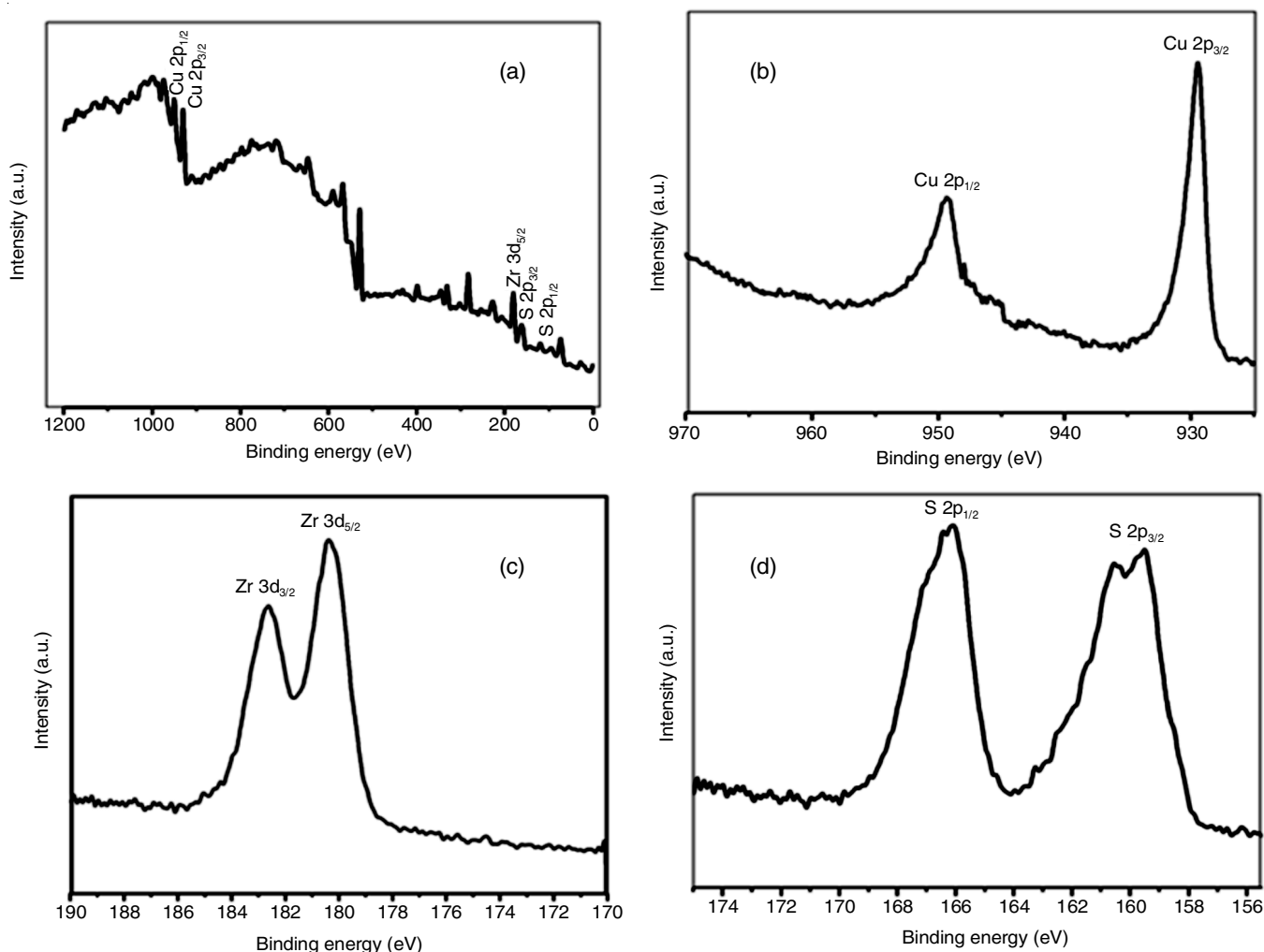
Fig. 2. XPS spectra of (0.1mM) CTAB stabilized CuS doped with Zr: nanostructures (a) full spectrum, (b) Cu 2p, (c) Zr 2p and (d) S 2p
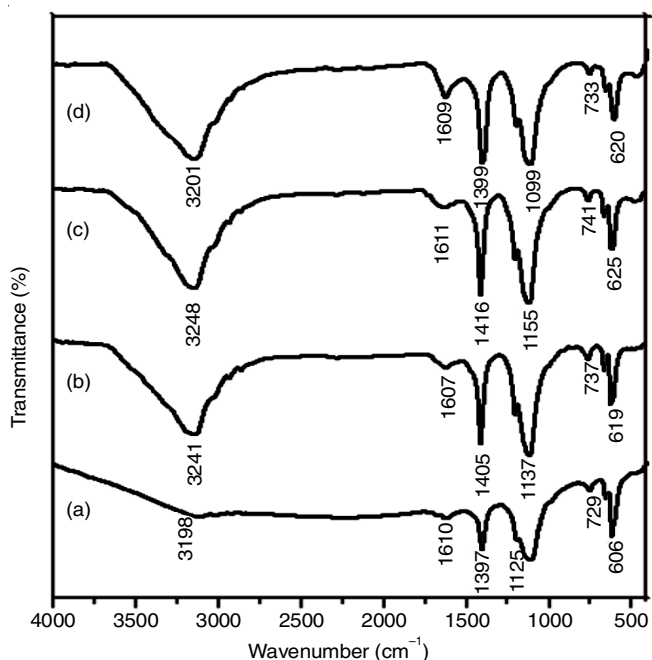

Fig. 3.   FTIR Spectra of (a) CTAB stabilized CuS (b) Zr (0.05) - CuS (c) Zr (0.15) - CuS and (d) (0.30) Zr-CuS nanostrutures

addition, the peaks at 1680-1460 cm^{-1} confirmed the Zr-CuS nanocomposites.

UV-Vis analysis: UV-Vis spectroscopy was performed to examine the optical property of as-synthesized Zr doped CuS and the results are reported in Fig. 4a-d. The as-synthesized Zr- doped absorption band at 496 nm is the characteristic band for the hexagonal structure of CuS [16]. The UV-vis spectrum for Zr doped CuS nano structures shows a significant change in the absorption spectrum due to the doping of Zr ions into CuS lattice. The observed results are almost similar to the reported literature [17]. The average optical transmission in the visible region decreased substantially at short wavelength mean the ultraviolet range. With increasing zirconium contents, an absorption edge shifted slightly to a longer wavelength region and the band gap also narrowed with increasing Zr contents. The crystallinity increases with an increase of Zr concentration may be the reason for more transmittance. The doping of Zr in the CuS changes the properties of CuS significantly.

Surface morphological analysis (SEM/EDS and TEM): The morphology of CuS and Zr-CuS powders has been investigated by SEM and the images are presented in Fig. 5a-l. Fig 5a-b the surface image of CTAB stabilized CuS powder that has an agglomerated sphere like structure. When zirconium is
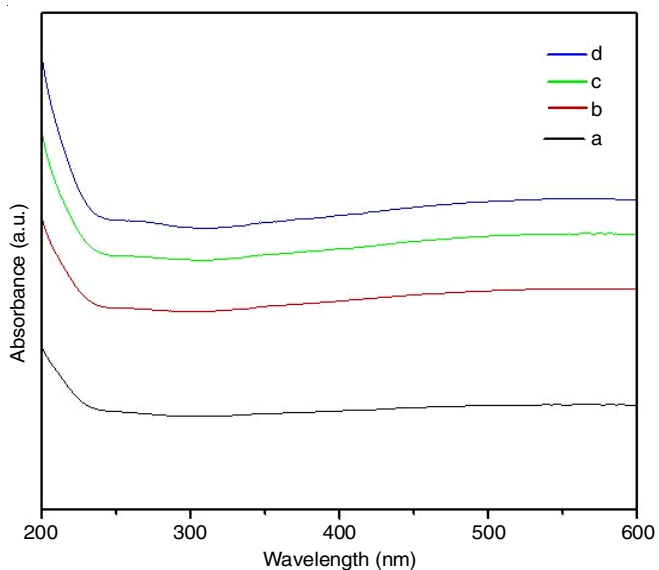
Fig. 4.   UV- Visible absorption spectra of (a) CTAB stabilized CuS (b) Zr (0.05) - CuS (c) Zr (0.15) -CuS and (d) (0.30) Zr-CuS nanostructures

doped on CuS, a few bundled flaky structures were observed. The nanostructures have formed because of nucleation and growth process with diameter of 25 nm. The EDS spectra of Zr doped CuS are shown in Fig. 5(c,f,i,l), which reflects that Zr^{2+} guest atoms have entered in the CuS crystal matrix. It is expected that Cu^{2+} ions will replaced the S^{2-} ions instead of occupying the interstitials. The doping levels and the bonding characteristics were determined by EDS spectrum.

Fig. 6a-c show the typical TEM images of Zr-doped CuS nanocomposite. It is noticed that the nanoparticles are quite monodisperse and uniform in size. Induced a slight variation in the reaction condition by dopent (zirconium) rendered smaller sized Zr-CuS nanocomposites. On the surface of CuS, the hydroxyl groups of ethylene glycol act as anchors and provides an excellent micro environment for the nucleation and growth of smaller sized zirconium doped CuS nanocomposites.

The diameter of the particles is about only 5-20 nm and has a mean value at 15 nm. There is significant morphological difference between CuS and Zr-CuS. The presence of Cu, Zr
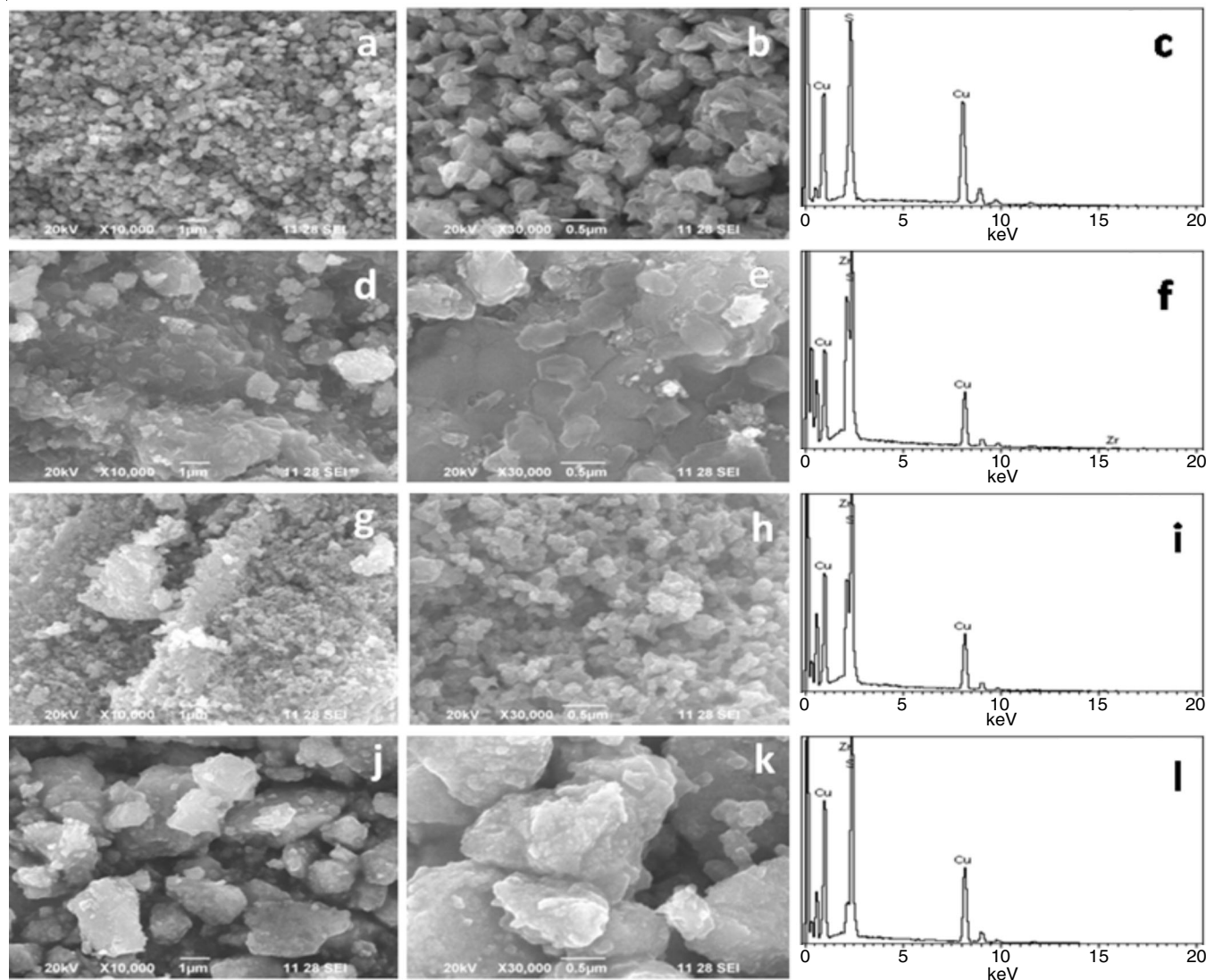

Fig. 5.   SEM images of (a,b) (0.1 mM) CTAB stabilized CuS, (d, e) (0.05) Zr-CuS, (g, h) (0.15) Zr-CuS, (j, k) (0.30 mM) Zr-CuS nanostructures and (c, f, i, l) are corresponding EDX spectra
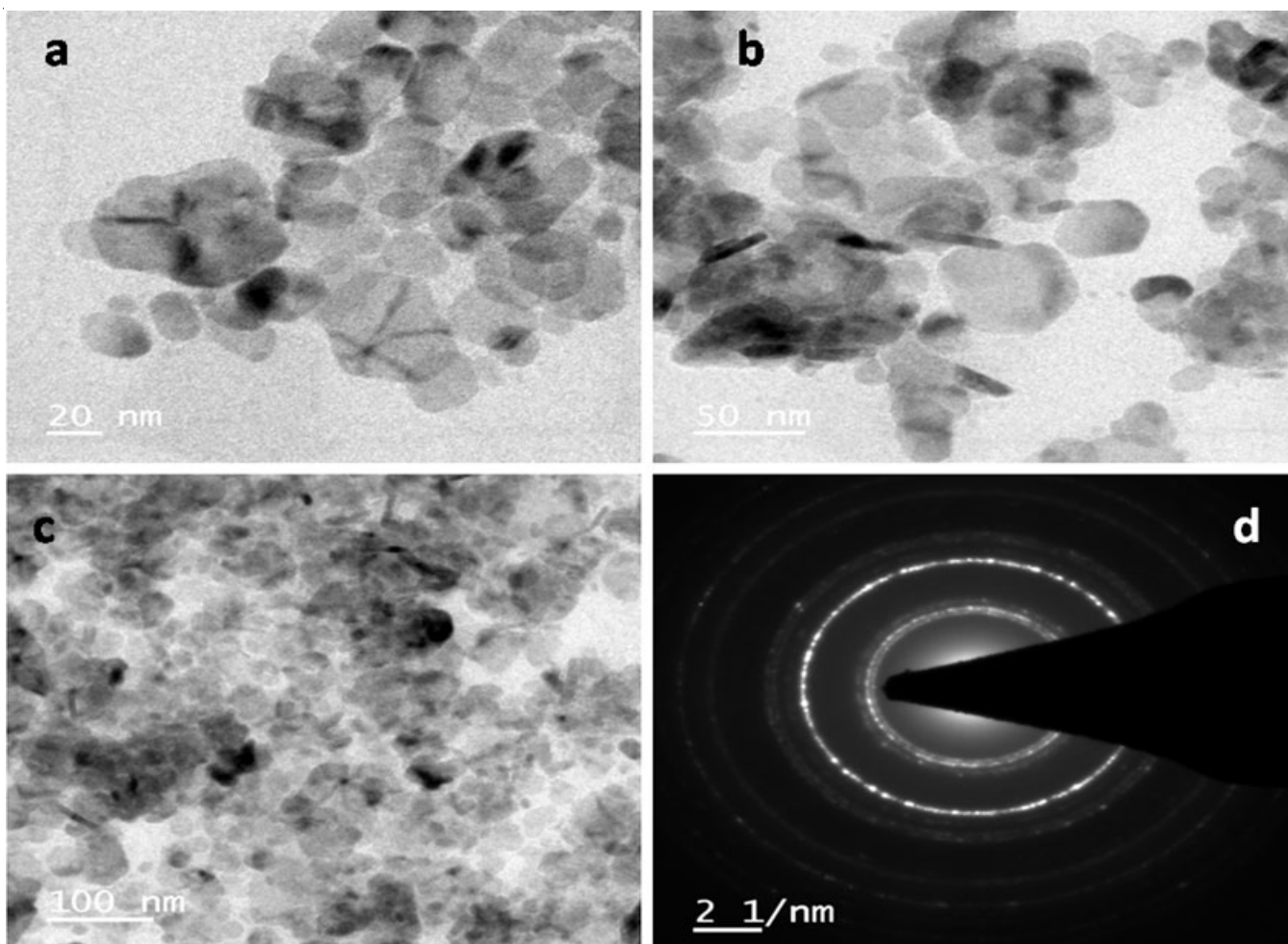
Fig. 6. (a)-(c) TEM images of (0.1 mM) CTAB stabilized Zr (0.05 mM) doped CuS nanostructures (d) SAED pattern of Zr doped CuS nanostructure

and S can be further confirmed in the XRD, XPS and EDS results. There is significant morphological difference between CuS and Zr-CuS, The hexagon Zr-CuS sheets may be held by weak van der Waals forces. The precursors concentration, reaction condition and sulfur source are some other structure promoting factors. Fig. 6c shows a SAED pattern of 0.05 mM Zr-CuS with ordered array of hexagonal spot, which confirms the formation of hexagon Zr-CuS and indication of the crystallinity.

Cyclic voltammetry: The cyclic voltammetric analysis were carried out using three electrode systems in 2 M KOH as electrolyte at different sweep rates (5, 10, 20 and 50 mV s^{-1}), which revealed good electrochemical behaviour. Fig. 7a shows the cyclic voltammogram of CTAB stabilized CuS with two consecutive weak oxidation peaks appeared at 3.0 V and 3.5 V, while a single and strong reduction peak was observed at 2.4 V. The reduction peak increases with the root mean square of the scan rate confirming a diffusion controlled process [18].

The capacitance of the materials increases linearly with increasing scan rate. Notably dispersion of zirconium on CuS, the voltammogram clearly shows sharp reduction peaks broadened, which vary at a scan rate of 50 mV/s. An increase in the capacitance shows that the electron transfer process occuring at Zr-CuS nanocomposite electrode is a surface confirmed

process. The specific capacitance of the sample CuS and Zr-CuS can be calculated by the following equation:

$$Cs = \frac{Q}{\Delta V.m} = \frac{I \times \Delta t}{\Delta V \times m} \tag{1}$$

where Cs is the specific capacitance, I is the current during discharge process, Δt is the discharge time, ΔV is the potential window and m is the mass of the active material.

Based on eqn. 1, the specific capacitance of CuS and Zr doped CuS electrode were quantified to be 949.47 F g^{-1} at 5 mV s^{-1} scan rate which is higher than that of CuS electrodes 328 F g^{-1} at 5 mV s^{-1}. In electrodes, the specific capacitance (Cs) decreased severely with increasing scan rate, which is attributed to the diffusion effect limiting the diffusion and migration of the electrolyte ions within the electrode. When increasing the scan rate, the transfer of ions becomes slow. During redox process the outer surface of the electrode material used for charge storage, meantime the capacitance decreases. Porous structure of nanomaterials can significantly develop utilization and specific capacitance of active electrode materials for supercapacitor.

Initially, the concentration of zirconium increases, the electrode current peak increases as well due to specific surface area of the nanocomposite. After the optimum Zr concentra-
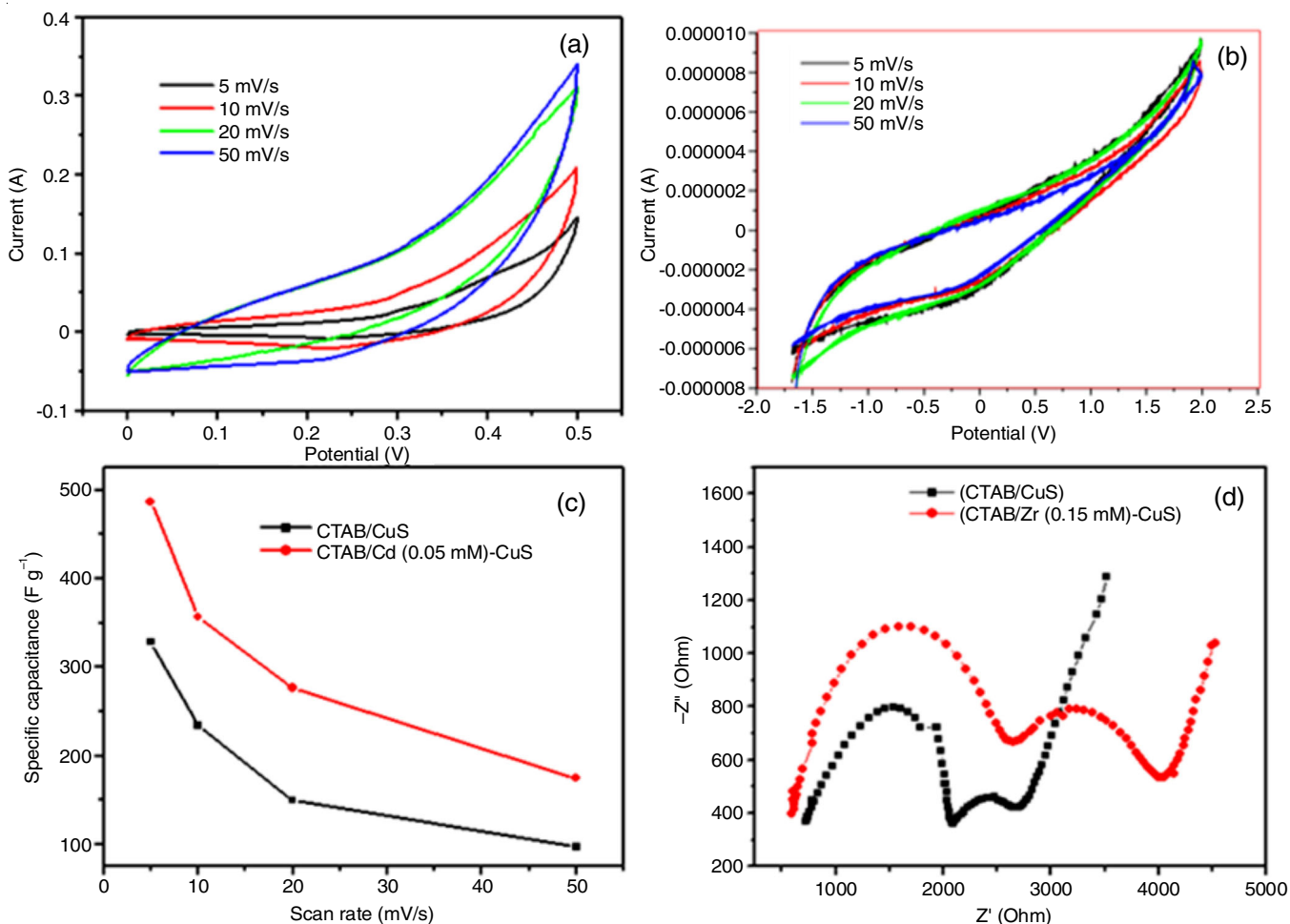
Fig. 7. Electrochemical characterization of two modified electrodes (a) CV curves of CTAB/CuS, (b) CTAB/Zr (0.05 mM)-CuS electrode at different scan rates, (c) Nyquist plots of modified CuS and Zr (0.05 mM)-CuS electrode

tion, the current peak decreases which causes the lower capacitance. This reduction in the current peak may be due to electrode resistance. Ion size and diffusion of anions and cations are important parameters for specific capacitance calculation. Conway and Pell [19] reported that a derivation in the cyclic voltammogram from classical square waveform due to resistance effects. Pore resistance is another important parameter affecting the capacitance in high sweep rates. When an increase in the sweep rate, loss of energy is high and the surface is less which leads to the decrease in the capacitance.

The capacitance of the active electrode material increases linearly with increase in the scan rate. For comparison, a capacitance of CTAB-CuS and CTAB-CuS doped with zirconium was measured (Fig. 7a-b). Notably, the cyclic voltammograms showed a significant difference. The change in the shape of the redox peaks at different scanning speeds indicates the conductivity of electrode material in 2 M KOH electrolyte. The broad redox peak in Zr-CuS at 5 mV clearly indicates the better capacitance of the nanocomposite [20]. The enhanced capacitance shows the electron transfer process is happing in Zr-CuS nanocomposite electrode is definitely surface confined process.

Electrochemical impedance spectroscopic analysis was carried out using a frequency range of 10^5 to 10^{-1} Hz in 2 M KOH,

using three electrode cells connected to an electrochemical station. A Zr-CuS sample acted as the working electrode in the three electrode system. This study demonstrates the electron transfer phenomenon across the sample and electrolyte interface.

Nyquist plot (Fig. 7d) of Zr-CuS reveals that a semi-circular curve (high frequency) and an inclined straight line (low frequency) represents AC impedance curve for the ideal capacitance. The diameter of the semicircle representing the charge transfer resistance, which is associated with the porous nature of the electrode material [21]. Warburg impendence (inclined straight line) is characterized by its real and imaginary contributions of impedance, which leads to form a phase angle 45°. The diameter of the semi-circle in the high frequency region represents the charge transfer resistance, which is associated with the pore structure of the material. The point of intersecting with the real axis of Nyquist curves is equivalent series resistance. It indicates the total resistance of the electrode, the bulk electrolyte resistance and the resistance at eletrolyte/eleclode interface [22]. The electrochemical characteristics of the as-prepared Zr doped CuS nanocomposites and previously reported nanocomposites are compared (Table-1). It is found that the specific capacitance of the as prepared nanocomposite is highly better than other reported nanocomposites.

TABLE-1
COMPARISON OF SPECIFIC CAPACITANCE
WITH EARLIER REPORTS

Electrode materials	Specific capacitance (F g⁻¹)	Method of preparation	Ref.
Carbon-ZrO_2	180.00	Hydrothermal	[23]
ZrO_2/Carbon block	43.20	Hydrothermal	[24]
ZrO_2-SiO_2/WO_3	313.00	Solgel	[25]
CTAB/CuS	328.26	Hydrothermal	[26]
Zr-CTAB-CuS	949.47	Hydrothermal	Present work

Conclusion

In this work, a CTAB stabilized CuS and hexagonal Zr doped CuS nanocomposites were synthesized by a simple hydrothermal route. The final products were characterized by XRD, XPS, FTIR, SEM/EDS and TEM. During the syntheses, the CTAB has played a significant effect as a stabilizer and zirconia as structure modifier with an average grain size of 10-25 nm. The nanocomposite has demonstrated enhanced electrochemical properties. The Zr-CuS nanocomposite has demonstrated enhanced electrochemical properties. The prepared electrode with Zr-CuS has a maximum capacitance value of 949.47 F/g. Sample with an optimum combination of an adequate micro-mesopore network, pore width and amount of zirconia on CuS is the best measures for energy storage. The present investigation strongly suggests the usage of zirconia doped CuS composites as electrode materials in next-generation pseudocapacitors.

CONFLICT OF INTEREST

The authors declare that there is no conflict of interests regarding the publication of this article.

REFERENCES

1. A.C. Pierre and G.M. Pajonk, *Chem. Rev.*, **102**, 4243 (2002);
https://doi.org/10.1021/cr0101306
2. P.H.C. Camargo, K.G. Satyanarayana and F. Wypych, *Mater. Res.*, **12**, 1 (2009);
https://doi.org/10.1590/S1516-14392009000100002
3. Z. Lu, Z. Zhu, X. Zheng, Y. Qiao, J. Guo and C.M. Li, *Nanotechnology*, **22**, 155604 (2011);
https://doi.org/10.1088/0957-4484/22/15/155604
4. K. Tomishige, Y. Furusawa, Y. Ikeda, M. Asadullah and K. Fujimoto, *Catal. Lett.*, **76**, 71 (2001);
https://doi.org/10.1023/A:1016711722721
5. T. Chraska, A.H. King and C.C. Berndt, *Mater. Sci. Eng. A*, **286**, 169 (2000);
https://doi.org/10.1016/S0921-5093(00)00625-0
6. H. Mudila, S. Rana and M. Zaidi, *J. Anal. Sci. Technol.*, **7**, 3 (2016);
https://doi.org/10.1186/s40543-016-0084-7
7. D.J. Guo, X.P. Qiu, W.T. Zhu and L.Q. Chen, *Appl. Catal. B*, **89**, 597 (2009);
https://doi.org/10.1016/j.apcatb.2009.01.025
8. J.W. Brown, P.S. Ramesh and D. Geetha, *Mater. Res. Express*, **5**, 024007 (2018);
https://doi.org/10.1088/2053-1591/aaad55
9. G.D. Wilk, R.M. Wallace and J.M. Anthony, *J. Appl. Phys.*, **89**, 5243 (2001);
https://doi.org/10.1063/1.1361065
10. K.K. Srivastava, R.N. Patil, C.B. Choudhary, K.V.G.K. Gokhale and E.C. Subbarao, *Trans. J. Br. Ceram. Soc.*, **73**, 85 (1974).
11. P. Surekha, D. Geetha and P.S. Ramesh, *J. Mater. Sci.: Mater. Electron*, **28**, 15387 (2017);
https://doi.org/10.1007/s10854-017-7424-2
12. Y.X. Bai, J.J. Wu, X.P. Qiu, J.Y. Xi, J.S. Wang, J. Li, W. Zhu and L. Chen, *Appl. Catal. B*, **73**, 144 (2007);
https://doi.org/10.1016/j.apcatb.2006.06.026
13. J. Nair, P. Nair, F. Mizukami, Y. Oosawa and T. Okubo, *Mater. Res. Bull.*, **34**, 1275 (1999);
https://doi.org/10.1016/S0025-5408(99)00113-0
14. G. Colon, M.C. Hidalgo, G. Munuera, I. Ferino, M.G. Cutrufello and J.A. Navio, *Appl. Catal. B*, **63**, 45 (2006);
https://doi.org/10.1016/j.apcatb.2005.09.008
15. S. Zhou, G. Garnweitner, M. Niederberger and M. Antonietti, *Lagmuir*, **23**, 9178 (2007);
https://doi.org/10.1021/la700837u
16. L.Z. Pei, L.J. Yang, J.F. Wang, C.G. Fan and J.L. Hu, *J. Surf. Sci. Nanotechnol.*, **8**, 384 (2010);
https://doi.org/10.1380/ejssnt.2010.384
17. A.E. Raevskaya, A.L. Stroyuk, S.Y. Kuchmii and A.I. Kryukov, *J. Mol. Catal. A*, **212**, 259 (2004);
https://doi.org/10.1016/j.molcata.2003.11.010
18. S. Hara and M. Miyayama, *Solid State Ion.*, **168**, 111 (2004);
https://doi.org/10.1016/j.ssi.2004.01.030
19. B.-E. Conway and W.G. Pell, *J. Power Sources*, **105**, 169 (2002);
https://doi.org/10.1016/S0378-7753(01)00936-3
20. K. Gurushantha, K.S. Anantharaju, L. Renuka, H.P. Nagaswarupa, S.C. Sharma, S.C. Prashantha, Y.S. Vidya and H. Nagabhushana, *RSC Adv.*, **7**, 12690 (2017);
https://doi.org/10.1039/C6RA25823A
21. D. Hulicova-Jurcakova, M. Seredych, G.Q. Lu and T.J. Bandosz, *Adv. Funct. Mater.*, **19**, 438 (2009);
https://doi.org/10.1002/adfm.200801236
22. Y. Zhang, H. Feng, X. Wu, L. Wang, A. Zhang, T. Xia, H. Dong, X. Li and L. Zhang, *Int. J. Hydrogen Energy*, **34**, 4889 (2009);
https://doi.org/10.1016/j.ijhydene.2009.04.005
23. A. Elmouwahidi, E. Bailon-Garcia, A.F. Perez-Cadenas, F.J. Maldonado-Hodar, J. Castelo-Quiben and F. Carrasco-Marin, *Electrochim. Acta*, **259**, 803 (2018);
https://doi.org/10.1016/j.electacta.2017.11.041
24. M. Nasibi, M.A. Golozar and G. Rashed, *J. Power Sources*, **206**, 108 (2012);
https://doi.org/10.1016/j.jpowsour.2012.01.052
25. G.H. Jeong, H.-M. Lee, J.-G. Kang, H. Lee, C.-K. Kim, J.-H. Lee, J.-H. Kim and S.-W. Kim, *Appl. Mater.*, **6**, 20171 (2014);
https://doi.org/10.1021/am505747w
26. D. Geetha, P. Surekha and P.S. Ramesh, *J. Mater. Sci.: Mater. Electron.*, **28**, 15387 (2017);
https://doi.org/10.1007/s10854-017-7424-2